Available online at www.sciencedirect.com
SCIENCE DIRECT®
ELSEVIER
Nuclear Instruments and Methods in Physics Research A 552 (2005) 409–419
NUCLEAR INSTRUMENTS & METHODS IN PHYSICS RESEARCH Section A
www.elsevier.com/locate/nima

Beam tests of the balloon-borne ATIC experiment

O. Ganel[a,*], J.H. Adams Jr.[b], H.S. Ahn[a], J. Ampe[b], G. Bashindzhagyan[c], G. Case[d], J. Chang[e,h], S. Ellison[d], A. Fazely[f], R. Gould[d], D. Granger[d], R. Gunasingha[f], T.G. Guzik[d], Y.J. Han[g], J. Isbert[d], H.J. Kim[g], K.C. Kim[a], S.K. Kim[g], Y. Kwon[g], M. Panasyuk[c], A. Panov[c], B. Price[d], G. Samsonov[c], W.K.H. Schmidt[e], M. Sen[d], E.S. Seo[a], R. Sina[a], N. Sokolskaya[c], M. Stewart[d], A. Voronin[c], D. Wagner[b], J.Z. Wang[a], J.P. Wefel[d], J. Wu[a], V. Zatsepin[c]

[a]*Institute for Physical Science and Technology, University of Maryland, College Park, MD 20742, USA*
[b]*NASA Marshall Space Flight Center, Huntsville, AL 35812, USA*
[c]*Skobeltsyn Institute of Nuclear Physics, Moscow State University, Moscow 119899, Russia*
[d]*Department of Physics and Astronomy, Louisiana State University, Baton Rouge, LA 70803, USA*
[e]*Max Planck Institut fur Aeronomie, D-37191 Katlenburg-Lindau, Germany*
[f]*Department of Physics, Southern University, Baton Rouge, LA 70813, USA*
[g]*Department of Physics, Seoul National University, Seoul 151-742, South Korea*
[h]*Purple Mountain Observatory, Chinese Academy of Sciences (CAS), China*

Received 9 April 2005; received in revised form 23 June 2005; accepted 26 June 2005
Available online 26 July 2005

Abstract

The Advanced Thin Ionization Calorimeter (ATIC) balloon-borne experiment is designed to perform cosmic-ray elemental spectra measurements from 50 GeV to 100 TeV for nuclei from hydrogen to iron. These measurements are expected to provide information about some of the most fundamental questions in astroparticle physics today. ATIC's design centers on an 18 radiation length (X_0) deep bismuth germanate (BGO) calorimeter, preceded by a $0.75\lambda_{\text{int}}$ graphite target. In September 1999, the ATIC detector was exposed to high-energy beams at CERN's SPS accelerator within the framework of the development program for the Advanced Cosmic-ray Composition Experiment for the Space Station (ACCESS). In December 2000–January 2001 and again in December 2002–January 2003, ATIC flew on the first two of a series of long-duration balloon (LDB) flights from McMurdo Station, Antarctica. We present here results from the 1999 beam tests, including energy resolutions for electrons and protons at several beam energies from

*Corresponding author. Tel.: +1 301 405 4857; fax: +1 301 314 9363.
E-mail address: opher@umd.edu (O. Ganel).

0168-9002/$ - see front matter
doi:10.1016/j.nima.2005.06.081

100 to 375 GeV as well as signal linearity and collection efficiency estimates. We show how these results compare with expectations based on simulations and their expected impacts on mission performance.

PACS: 07.20.Fw; 07.77.Ka; 07.87.+v; 95.55.Vj

Keywords: Cosmic-ray calorimeter; High-energy cosmic rays

1. Introduction—science objectives

For nearly a century, high-energy charged particles from outer space have been known to constantly hit the Earth's atmosphere. These 'cosmic-ray' particles follow a remarkably uniform power-law spectrum over more than 10 orders of magnitude in energy. Above about 10^{10} eV cosmic-ray particles are extra-solar, and believed to be accelerated at supernova shocks. The widely accepted supernova remnant (SNR) model predicts that at or near $Z \times 10^{14}$ eV, this acceleration mechanism reaches a cutoff [1]. Despite this, ground-based arrays of cosmic-ray detectors have detected particles with reconstructed energies in excess of 10^{20} eV [2,3]. Particles with energies above 10^{18} eV are believed to be of extra-galactic origin [4], possibly accelerated by active galactic nuclei (AGN) [5,6]. Ground-based measurements do not record the primary cosmic-ray nucleus, but rather measure the shower it induces in the Earth's atmosphere. Charge identification of the primary is thus deduced in a model-dependent fashion. The only practical way to reliably measure the incident charge is to make direct measurements prior to the start of the shower by use of detectors flown at the top of the atmosphere or in low Earth orbit. Reliable measurement of particle energy for H and He nuclei above about 10^{12} eV requires the use of a calorimeter. Model-independent elemental spectral measurements would provide crucial hints as to the source of cosmic-ray particles, their acceleration mechanism and propagation through the interstellar medium.

ATIC (Fig. 1) is a balloon-borne instrument comprised of several detector systems (calorimeter, scintillator hodoscopes and a silicon matrix charge detector) intended to measure the charge (or identity) of incident cosmic-ray nuclei and their energy. From these measurements, one can extract the spectra of nuclei from H to Fe in the energy range 5×10^{10}–10^{14} eV [7,8].

2. The ATIC detector

An experiment's science objectives and basic detection technique determine its measurement objectives. These measurement objectives then drive the detector design. For flight detectors, there are several unique constraints that must be taken into account in addition to the measurement objectives. The weight a balloon can lift is limited, with instrument weights usually up to 1–1.5 tons allowed. Power generation typically depends on solar arrays, limiting instrument power to several hundred watts continuous dissipation. Depending on the type of detector, data rates may require a greater bandwidth than that available through telemetry. In such cases, data must be archived onboard on disk or tape, which may limit the trigger rate and/or the size of the average event record. To enable its science objectives, ATIC must measure incident particle charge with a resolution of 0.2 charge units, with misidentification due to back-scatter no greater than 3% [9]. Incident energy must be measured with a resolution of $<50\%$ and preferably with no non-Gaussian high-end tails. Incident particle trajectory must be reconstructed accurately enough to allow accurate charge measurement by identifying the pixel in the charge detector that the primary traversed.

To achieve its measurement objectives, ATIC is comprised of an $18X_0$ deep, fully active BGO calorimeter, preceded by $\sim 0.75\lambda_{\mathrm{int}}$ graphite target section to induce nuclear interactions of incident particles before entering the calorimeter (for

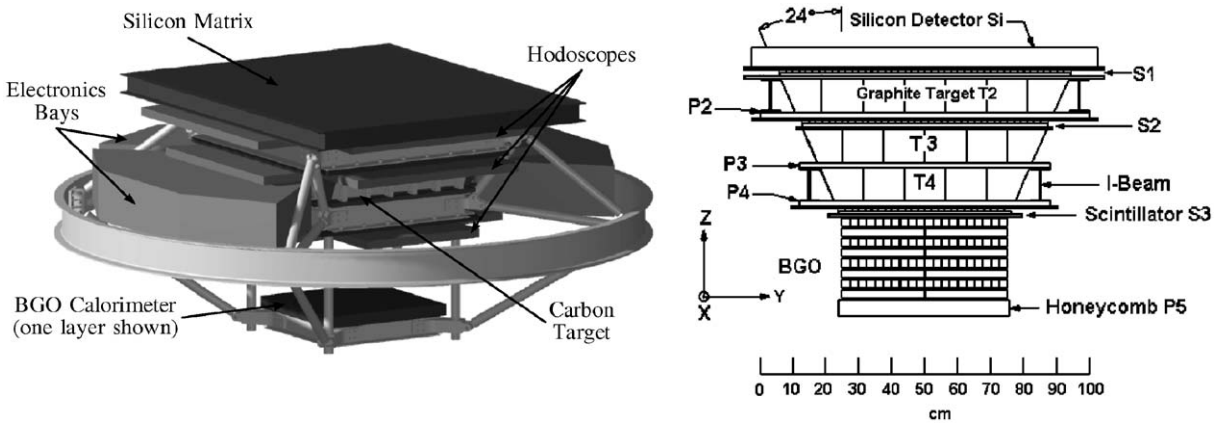

Fig. 1. 3D mechanical drawing (left) and 2D simulation schematic (right) of the ATIC configuration.

~53% of protons and a higher fraction of heavier nuclei). A matrix of Si pixels [10] is utilized to measure incident charge, with scintillator hodoscopes interleaved with the graphite layers to provide a fast trigger and enhance track reconstruction accuracy needed to correctly identify the pixel traversed by the primary. Use of a low-Z target material, such as graphite, increases the effective collection power (geometry factor or GF) of ATIC while minimizing the weight impact. Given the relatively loose energy resolution requirement, a thin calorimeter is indicated. Such a detector weighs less than a full-depth (e.g. $10\lambda_{\mathrm{int}}$) one while maximizing the GF by allowing high-angle incidence. The total instrument weight as flown was about 3400 lb, including about 780 lb of BGO.

The ATIC calorimeter is comprised of eight layers (ten layers at the beam test) of fully active, laterally oriented BGO crystals, each $2.5 \times 2.5 \times 25.0\,\mathrm{cm}^3$. For mechanical reasons, the crystals are held in trays, with 20 crystals in each half-tray, for a lateral layer dimension of $50.3 \times 50.3\,\mathrm{cm}^2$. The inert material in the calorimeter comprises about 1.7% of its depth in radiation lengths ($0.3X_0$ out of $17.8X_0$). Hamamatsu R5611 photo-multiplier tubes (PMTs) read out each crystal separately with three dynode pickoffs for extended linear dynamic range (for single-crystal energy deposits from 10 MeV up to 20 TeV). Above the calorimeter is a 3-layer graphite target shaped as an inverted truncated pyramid with a 24° opening angle. Three scintillator-strip hodoscopes are located above the target (S1), under the top graphite layer (S2) and above the BGO (S3). Each hodoscope is comprised of a crossed pair of layers with 42 (S1), 35 (S2), or 24 (S3), 2 cm wide, 1 cm thick strips, each read out (two ranges to cover 0.5–800 MeV) from both ends by the same Hamamatsu R5611 PMTs used in the calorimeter. Above the top hodoscope is a matrix of $1.945 \times 1.475\,\mathrm{cm}^2$ Si pixels arranged in sets of four pixels per detector, 28 detectors per motherboard, two motherboards per ladder and 20 ladders overall. In flight, the Si matrix covers $\sim 1 \times 1\,\mathrm{m}^2$. At the beam test, only 40 detectors of each of the three central ladders were populated.

The calorimeter measures the energy of incident protons and nuclei mostly through the electromagnetic component of their shower. The calorimeter depth (~0.91 nuclear interaction lengths or $17.8X_0$ in flight; ~1.14 interaction lengths or $22.3X_0$ at the beam test) determines the energy response, defined here as the ratio of the measured energy to the particle's incident energy, as most of the hadronic component of the shower (mainly charged pions) escapes through the bottom and sides of the calorimeter. This depth also determines energy resolution, i.e. the uncertainty in the energy measurement, due to fluctuations in the

fraction of shower energy carried by the electromagnetic component. Energy resolution is usually calculated as the ratio of the width (RMS or, as in this paper, standard deviation—σ) and the mean value for the measured energy distribution for a given incident energy. The calorimeter's lateral segmentation allows reconstruction of the shower axis, pointing back to the primary particle's point of incidence on the Si matrix. The Si matrix is used to measure incident particle charge (up to Fe), with its fine segmentation minimizing the impact of back-scattered shower particles on that measurement.

3. ATIC electronics

Calorimeter and hodoscope PMTs are read out using Application Specific Integrated Circuits (ASICs) developed for the ACE space mission. These 16-channel chips utilize charge-sensitive amplifiers and on-chip 12bit Wilkinson ADCs. Each channel can be triggered when the signal exceeds one of the two adjustable thresholds. For the calorimeter, with three separate signals measured for each PMT, this implies up to six available trigger thresholds. For the hodoscopes, with two signals per PMT, four trigger levels are available. Six ACE ASICs are mounted on each front-end module (FEM), with each chip digitizing signals from one range for either a quarter calorimeter layer or a third of a hodoscope layer (one side). In the beam test configuration, three hodoscope FEMs were connected to a single hodoscope ASIC Control Logic Board (ACLB), and five calorimeter FEMs were connected to a single calorimeter ACLB. Two hodoscope ACLBs and two calorimeter ACLBs were connected to a single Detector Interface Module (DIM). There were two DIMs, each responsible for the hodoscope and calorimeter data from two adjacent sides of ATIC. The Si matrix is read out using CR-1.4 ASICs [12]. These 16-channel chips have charge-sensitive amplifiers, shapers and sample-and-hold circuits. Seven CR-1.4 chips are mounted on a single motherboard (MB), each reading out the 16 pixels of four Si pads. The signals from the seven chips are multiplexed onto a common data line to a grandmotherboard (GMB). Each GMB supports 10 MBs, digitizing the analog CR-1.4 signals and placing them in output registers. From the output registers, the signals are read by ACLBs (two per GMB) and compared to pedestals measured for the appropriate pixels. Signals exceeding the pedestal by an adjustable amount are buffered into the data system. This 'data sparsification' reduces Si matrix data size for the average event by two orders of magnitude. The GMBs also periodically calibrate each channel with known charge pulses, one ACLB at a time.

The ATIC trigger system includes a fast pretrigger (PT) based on signals from the hodoscopes exceeding adjustable thresholds, and as a second level, a master trigger (MT) based on signals from the BGO exceeding adjustable thresholds. Trigger logic is controlled by the control logic module (CLM), which includes an Actel gate array. This gate array is programmed with the algorithms developed through simulation studies to provide non-biased, high-efficiency triggers, while maintaining the trigger rate low enough to ensure the data collected in a flight fits on the onboard hard disks. The instrument is controlled via a command system which allows remote commanding including simple commands and command macro activation, as well as local commands initiated by the onboard processors. A housekeeping system monitors various temperature and pressure sensors, as well as voltages, currents, software status, etc. ATIC is encased in a Kevlar pressure vessel pressurized to about 0.5 atm, greatly reducing the probability of high voltage arcing without resorting to potting of all HV connections and improving thermal control. The 0.5 atm value provides these advantages while minimizing the risk of rupturing the pressure vessel.

4. ATIC data collection and processing

ATIC's Flight Data System (FDS) is comprised of several CPU nodes. The data is recorded by the FDS in binary format and transferred to a separate Ground Data System (GDS). From the

GDS, the data is distributed to member institutions for calibration and analysis. The binary files are read and processed using a ROOT-based[1] custom package—the ATIC Data Processing System (ADPS) [13,14]. ATIC data is sparsified by comparing signal levels in each channel for each event to a periodically updated database. This database holds values that are somewhat above the mean pedestal value for each electronic channel. Thus, only significant signals are recorded in the data stream, reducing the average event size. This system requires that each signal level be accompanied by a 16bit 'electronic address' that identifies the channel. At CERN, a complete mapping between the electronic channels and physical pixels, strips and crystals was used to generate a lookup table linking electronic addresses, physical addresses and physical location for each channel. The event records archived by the FDS constitute the ATIC raw data. After the end of a flight or a beam test, this raw data is time-ordered, bad blocks are removed, etc., producing the ATIC Level 0 (L0) data.

Pedestal values are calculated based on the data for each electronic channel at different times and recorded in pedestal lookup tables. Cosmic-ray muon distributions are plotted and fitted for each crystal, strip and pixel to calibrate the Si matrix and the low-range readouts of the calorimeter and scintillator hodoscopes. The inter-range calibrations for dynode pickoffs (low-, mid- and high-range for the BGO, and low- and high-range for the hodoscopes) are determined based on data from events with showers, where two ranges provided significant (but not saturated) signals. This process, with additional information gleaned from charge pulsers and LED flash events allows L0 data to be calibrated, translating ADC counts to physics units (such as MeV, etc.) and L0 data to Level 1 (L1) data. Using algorithms developed through simulation studies, the measured energy deposit patterns are interpreted to reconstruct the incident particle charge, energy and trajectory. This processing produces a Level 2 (L2) set of overall event parameters, which can then be used to reconstruct the energy spectra of different nuclei.

[1]ROOT [11] is a powerful, object-oriented, data analysis and presentation tool, featuring a C++ interpreter, user-defined classes, dynamic link-in of pre-compiled scripts and a powerful graphical user interface.

5. Beam test objectives and data collected

In September 1999, ATIC was placed in the H2 beamline of the Super Proton Synchrotron (SPS) at CERN (the European high-energy physics laboratory) and data was collected from proton, electron and pion beams at energies from 100 to 375 GeV. Between beam runs, ATIC collected cosmic-ray muon events for calibration purposes. The ATIC configuration during the beam test included 25 cm depth of BGO vs. 20 cm in the flight configuration (the flight configuration was truncated due to more stringent weight requirements than originally anticipated). Except for cosmic-ray muons, triggered by the ATIC PT, ATIC was triggered using a beam trigger comprised of external scintillator paddles and trigger electronics (provided by NASA/GSFC) to assure passage of precisely one particle per event.

This beam test was the first major test intended to validate the ATIC hardware and software. The beam test had several other major objectives including measurement of energy resolution and data collection efficiency. Since test beams at particle accelerator facilities can only provide proton energies up to several hundred GeV, or about two orders of magnitude short of ATIC's energy range, studies of the instrument's behavior at higher energies must be carried out using Monte Carlo simulations. By comparing simulation results to measurements at available energies, one can verify the precision of said simulations and assess their likely accuracy at higher energies. During a 1 week beam test period, ATIC collected proton data at 150 and 375 GeV in a grid covering most of the calorimeter, at angles of 0°, 15° and 30°. In addition, 150 GeV π^- data were collected with particles incident at the center of the calorimeter at angles of 0° and 30°. Electron data were also collected at 100, 150 and 300 GeV with similar grid positions and angles to those

of the proton runs. Absolute calibration was based on cosmic-ray muons collected with random incident positions and angles. Pedestal, charge-pulser and LED flasher events were collected both to facilitate calibration and test the relevant systems.

6. Calibration with cosmic-ray muons

Muons deposit energy in matter via the well-understood and accurately simulated electro-weak interaction. Accordingly, muons present an invaluable tool for inter-calibrating the different BGO crystals. Using the most probable energy deposit from muons in each crystal, gain corrections were calculated and used to equalize the low-energy range readout response. High-energy showers were used to inter-calibrate different readout ranges for the same crystal, by comparing the low- and mid-ranges or the mid- and high-ranges for those cases where two ranges registered activity and neither saturated. A similar procedure was used to inter-calibrate the low-energy range readout of hodoscope scintillator strips, and to inter-calibrate the low- and high-range readouts there.

7. Comparison of beam test data and simulations

Since the beginning of the ATIC project in 1994, proton showers in ATIC have been simulated using GEANT [15] with the FLUKA and GHEISHA models. Ultimately, FLUKA [16] was chosen as the more accurate model for the high energies of interest to the ATIC experiment. Protons showering in ATIC were simulated [17] with a variety of incident energies, and with a power-law spectrum (see Fig. 1 for the simulation model schematic). Various incident positions and angles were simulated, including random position and isotropically distributed angles, with typically 50,000 events for any combination of energy, position and angle. Simulation studies were carried out on topics such as distribution of secondary shower particles and back-scattered particles, energy deposit by back-scattered particles in charge detectors above the calorimeter and its dependence on the vertical separation between the detectors, lateral distance from incident particle trajectory, and target material. Track reconstruction algorithms were developed using the energy deposit pattern in the calorimeter alone, as well as in conjunction with the deposit patterns in the scintillator hodoscopes and/or in the silicon charge detector above the targets [18]. The expected charge misidentification fraction was studied for charge detectors comprised of various sizes of strips and of pixels [7]. The ATIC trigger model was developed and optimized. The expected sensitivity of the ATIC experiment to the break in the proton spectrum expected to be found at $\sim 10^{14}$ eV was also assessed. Based on the characteristics of the beams available at CERN, simulations were developed for the proper particle types, energies, incidence positions and angles and beam profile, with at least 2000 events per run type. These simulations have been used to compare with actual measurements.

A comparison between the measured energy deposit for electrons and the energy deposit expected from simulations validated the absolute energy calibration. Beam measurements for 150

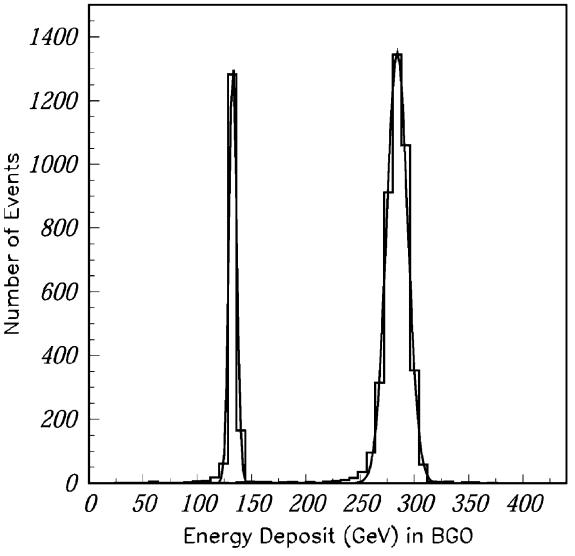

Fig. 2. Total BGO energy deposit (with Gaussian fit) for 150 GeV (left) and 300 GeV (right) electrons.

and 300 GeV electrons (Fig. 2) showed 91% containment of incident energy with a resolution of 2% at 150 GeV and 92% containment with 3% resolution at 300 GeV, where the containment fraction was defined as the ratio of the mean reconstructed energy to the nominal beam energy, and the resolution was defined as the ratio of the fit standard deviation to the fit mean, for both measured and simulated cases. Simulations predicted 92% containment and slightly better resolutions. The better resolutions in the simulations are the result of idealized conditions such as perfect readout digitization, perfect inter-crystal and inter-range calibration and no noise.

Proton data were collected mainly at 150 and 375 GeV. Fig. 3 shows the energy deposited by 150 and 375 GeV protons in the BGO calorimeter (data and simulation) following a simple event selection as follows:

1. At least one hit in the S1 scintillator hodoscope; AND
2. At least one hit in the S2 scintillator hodoscope; AND
3. At least one hit in the S3 scintillator hodoscope; AND
4. At least one crystal in the upper five layers of the BGO with more energy than expected from a non-interacting Be nucleus; AND
5. At least four consecutive BGO layers with significant shower activity or each of the 10 BGO layers with more energy deposit than expected from one minimum ionizing $Z = 1$ particle; AND
6. The sum of deposits in the uppermost scintillator layer less than the same sum in the lowest scintillator layer; AND
7. The sum of deposits in the uppermost BGO layer at least 30 times greater than the same sum in the uppermost scintillator layer.

Selection criteria 1 through 3 model the ATIC fast PT. Criteria 4 and 5 were meant to model the MT (ultimately in its first two flights ATIC used a simpler but essentially similar trigger model) with criterion 4 designed to remove the large background expected from H and He that do not interact at all or else interact too deep in the BGO to be measured well. Criteria 6 and 7 are meant to assure an inelastic interaction in the target. This 7-part selection retains about 62% of beam-trigger events. Once we account for the interaction

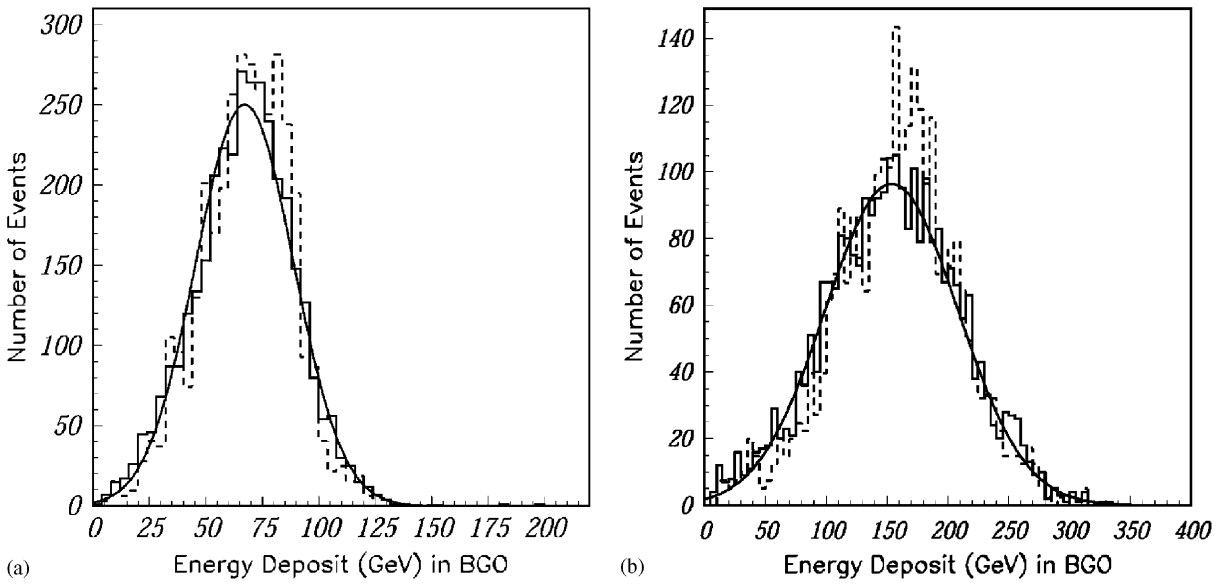

Fig. 3. BGO energy deposit for 150 GeV (left) and 375 GeV (right) protons incident at 30°—data (solid histogram and fit) and simulation (dashed histogram).

probability in the $0.75\lambda_{int}$ target, the efficiency for interacting events is found to be 85%. As stated above, the CERN run was intended to validate the ATIC hardware, software and simulations requiring data be collected over the entire surface of the detector, with various particle types, energies and incidence angles. The beam spot was very small compared to the size of the experiment requiring many runs taken at different grid points. Since ATIC was designed for a trigger rate of several tens of Hz as appropriate for a high-energy cosmic-ray detector of this size, the number of events that could be collected in the few days of beam time available was limited and needed to be allocated for the different types of runs. Only a limited data sample at any given point, energy and angle was needed to verify the proton line-shape, the calorimeter response for protons and the proton energy resolution, thus the several thousand events collected for that purpose (see Fig. 3) are quite sufficient.

Simulation reproduces the response and resolution reasonably well (simulated resolution is somewhat better for the same reasons explained above for electrons). The absence of any non-Gaussian high-end tail greatly simplifies ATIC's task of correctly measuring the spectral index of cosmic-ray particles. The longitudinal profiles of measured and simulated 150 GeV electron showers and 150 GeV proton showers are shown in Fig. 4. The proton simulation accurately reproduces the rising and falling slopes, the overall peak location and the energy deposited in the lowest calorimeter layers (indicating the leakage fraction of the shower's EM portion) of the experimental measurements. The simulated longitudinal profile for electrons rises somewhat more quickly than that of the beam data. This is most likely due to the higher graphite density in the simulations compared to the actual instrument (details in Section 8 below) increasing the amount of material before the BGO in the simulations by about 0.36 radiation lengths. Without this difference, the rising slope would rise slightly more slowly as the shower develops a little deeper in the BGO, causing the peak position to match more accurately that of the measured beam particles. This difference is much less important for proton shower profiles where the interaction occurs deep in the target and most of the EM particles do not travel significant distances in the graphite. A comparison of lateral proton shower profiles [19] shows the simulation reproduces the lateral energy deposit pattern at shower maximum down to less than 1% of the highest single-crystal deposit.

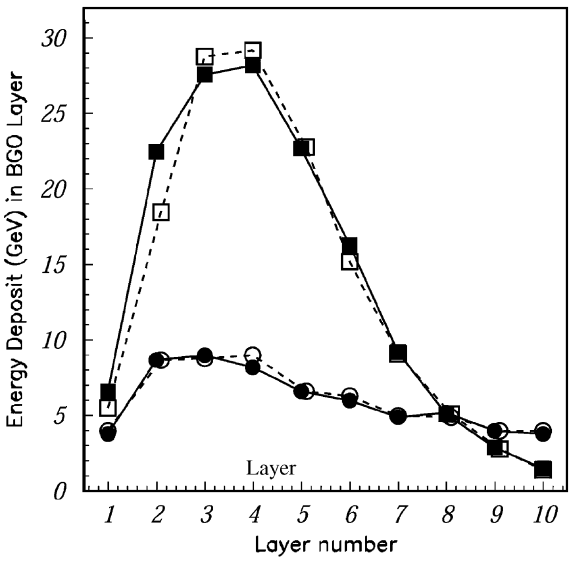

Fig. 4. Mean longitudinal profile of 150 GeV electrons (squares) and 150 GeV protons (circles)—data (open markers) and simulation (solid markers).

8. ATIC performance

In general, hadronic showers generate non-linear signals in most calorimeters. Depending on their composition and design, most calorimeters provide a higher signal per unit deposited energy for electromagnetic processes when compared to the same unit energy deposited through hadronic processes [20]. In full-depth (e.g. $8–10\lambda_{int}$) calorimeters, hadronic shower development tends to transfer an ever greater fraction of its energy from the hadronic component to the EM component for greater incident energy, as the number of hadronic interactions increases, each transferring a fraction (on average one-third) of its energy into π^0's that then decay into pairs of photons. With no corresponding process transferring energy from

the shower's EM component back to its hadronic component, the flow is uni-directional explaining the increase in the EM fraction. However, in thin ($\leqslant 2\lambda_{\mathrm{int}}$) calorimeters, where only the first interaction is contained in the calorimeter (with perhaps a fraction of the second-generation interactions), the *measured* EM energy fraction of a hadronic shower is almost energy-independent. As a result, calorimeters such as ATIC are nearly linear for hadrons, and their resolution is dominated by the energy-independent fluctuations in energy leakage caused by the event-to-event fluctuation in the EM energy fraction of those early interactions. While this situation determines that the energy resolution of such thin calorimeters for hadrons will be $>30\%$, the same effect tends to minimize energy-dependent systematic errors in energy reconstruction.

Cosmic-ray spectra are well described by power-law distributions over many decades of energy, with integrated fluxes falling by about a factor of 50 for an order of magnitude increase in threshold energy. With such rapidly falling spectra, Gaussian response curves greatly simplify reconstructing precise cosmic-ray spectral indices, as high-end tails would tend to reduce the apparent spectral slopes in the absence of proper corrections. Such corrections depend critically on full knowledge of the shape of any such tails and its dependence on incident particle energy. Given that the relationship of the measured energy to the incident energy itself depends on any tails, the analysis procedure required to correct for these is complicated. Fortunately, as seen in Fig. 3, ATIC avoids these complications.

Fig. 5 shows the energy (in)dependence of the response and the energy resolution for protons and electrons over the energy range available from the CERN beam tests. Unfortunately, accelerator beams are not available for much of ATIC's energy range, forcing us to depend on simulations to extrapolate up to 100 TeV. The beam test results are useful, however, for validating the accuracy of our simulations in the accelerator's energy range. The measured response is well reproduced by simulation (proton data 0.43 ± 0.02 vs. simulation 0.44 ± 0.01; electron data 0.92 ± 0.01 vs. simulation 0.91 ± 0.02). The measured proton resolutions (σ/μ) are compatible with an energy-independent value of $34\pm1\%$ (simulation predicts $29\pm2\%$). This small variation

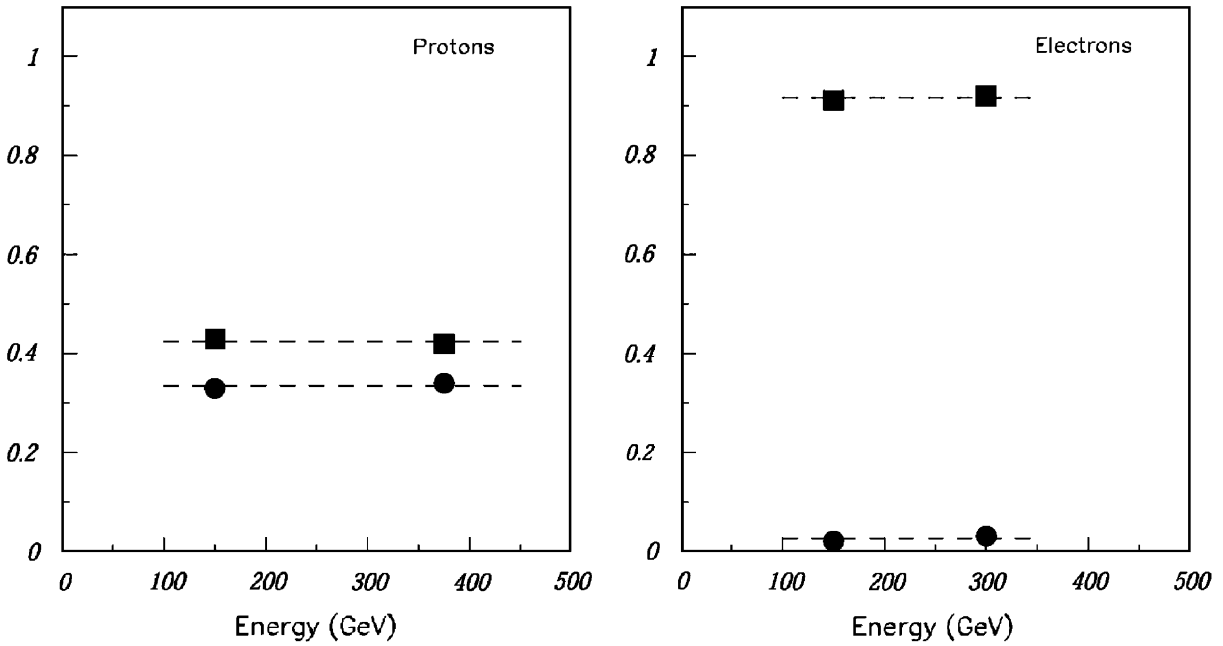

Fig. 5. Response (squares) and resolution (circles) vs. incident energy for beam protons (left) and electrons (right).

is due to several factors. First, the simulation program, started years before construction, assumes the book value for graphite density ($2.265\,g/cm^3$), vs. the actual density ($1.76\,g/cm^3$) of the industrial graphite ultimately used by ATIC. Simulations thus assume an increased likelihood of secondary shower particles interacting in the target, reducing the expected fluctuations of the measured signal. The simulation also does not include the multi-range, quantized readout utilized by ATIC to cover the large dynamic range (about six orders of magnitude), and assumes perfect calibration, causing it to underestimate the uncertainty in energy reconstruction. As shown in Fig. 3, the proton lineshape is nearly Gaussian. There are no physics processes known that would lead us to expect the accuracy of our simulations to degrade for higher incident proton energies within ATIC's expected range. Therefore, once our CERN data validated the simulation results over the energy range covered in the beam tests, we can expect a similar accuracy up to 100 TeV. Our simulation results predict that the energy resolution will be energy-independent up to 100 TeV, and that the response will be nearly so, making us confident that ATIC will perform as required to achieve our scientific objectives.

Another critical parameter, the collection efficiency, determines the size of the data sample ATIC collects during its flights. With a steeply falling spectrum, the highest energy ATIC can reach will be determined by the size of its collected data sample. The collection efficiency is comprised of the probability for the proton to interact in the graphite target, generating a shower, and the likelihood of such a shower event to pass the trigger and event selection. The measured collection efficiency is between 62% (150 GeV) and 66% (375 GeV). Simulations predict a higher efficiency (e.g. 73% at 150 GeV) but correcting for the lower graphite density (see above) reduces the interaction probability and brings the predicted value down to 65%. This accounts for most if not all the difference between simulation and experimental measurement. The minor remaining difference may be due to beam impurities (typically a few percent of beam particles may be charged mesons which have a longer interaction length, or muons that do not interact hadronically).

9. Conclusions

Designing an experiment to accurately measure the incident nucleus energy and charge at the top of the Earth's atmosphere is a challenging task. The ATIC team has designed such a detector and tested it at CERN in September 1999. The large variety of beam data collected has allowed the validation of ATIC hardware, software and simulations. These data were also used to debug minor hardware problems prior to flight operations. The energy resolutions, response, collection efficiency and measured shower profiles agree with simulation results, proving that the ATIC simulation model has sufficient fidelity to allow its use for designing reconstruction algorithms and interpreting flight data. To the limits of the available beam energies, response and resolution appear nearly energy independent, as expected, with no non-Gaussian high-end tails, promising a successful flight program. Since the beam tests, ATIC has flown on two LDB flights collecting a total of about 110 GB of data. Analysis results ([21,22]) support the above conclusions.

Acknowledgements

This work was supported at UMD by NASA Grant NAG5-5155; at LSU by NASA Grants NAG5-5064 and NAG5-5306 and the Louisiana Board of Regents; at MSFC under the Supporting Research and Technology Program of NASA's Office of Space Science; at MSU by the Russian Foundation for Basic Research Grants 99-02-16246 and 02-02-16545; at MPI by the exchange program between the Chinese Academy of Sciences in China and the Max-Planck-Society in Germany; and at SNU by the Ministry of Science and Technology of Korea Grant 00-I-01-04-A-028. We are grateful to CERN and the CMS collaboration for allowing us to use their facilities. We also thank N. Doble of CERN who provided us with beams of excellent quality, and J. Mitchell of NASA/GSFC who arranged our beam-time, provided the beam trigger and helped tune the beams.

References

[1] T.K. Gaisser, Cosmic Rays and Particle Physics, Cambridge University Press, Cambridge, 1990.
[2] N. Hayashida, K. Honda, M. Honda, et al., PRL 73 (1994) 3491.
[3] D.J. Bird, S.C. Corbato', H.Y. Dai, et al., Astrophys. J. 424 (1994) 491.
[4] N. Hayashida, et al., Astropart. Phys. 10 (1999) 303.
[5] P.L. Biermann, P.A. Strittmatter, Astrophys. J. 322 (1987) 643.
[6] G.R. Farrar, P.L. Biermann, PRL 81 (1998) 3579.
[7] E.S. Seo, J.H. Adams, G.L. Bashindzhagyan, et al., The advanced thin ionization calorimeter (ATIC) balloon experiment: expected performance, in: Proceedings of SPIE, vol. 2806, Denver, 1996, p. 134.
[8] T.G. Guzik, J. Adams Jr., J. Ampe, G. Bashindzhagyan, P. Boberg, et al., The advanced thin ionization calorimeter (ATIC) for studies of high energy cosmic rays, in D. Kieda, M. Salamon, B. Dingus, (Eds.), Proceedings of the 26th ICRC, vol. 5, Salt Lake City, 1999, p. 9.
[9] E.S. Seo, et al., Adv. Space Res. 19 (5) (1997) 711.
[10] J.H. Adams, et al., Silicon matrix detector for ATIC, in: Proceedings of the 26th ICRC, vol. 5, Salt Lake City, 1999 p. 76.
[11] R. Brun, F. Rademakers, Nucl. Instr. and Meth. A 389 (1997) 81.
[12] J.H. Adams, et al., The CR-1 chip: custom VLSI circuitry for cosmic rays, in: Proceedings of the 26th ICRC, vol. 5, Salt Lake City, 1999, p. 69.
[13] O. Ganel, et al., Data processing and event reconstruction for the ATIC balloon payload, in: Proceedings of the 26th ICRC, vol. 5, Salt Lake City, 1999, p. 43.
[14] H.S. Ahn, et al., ATIC flight data processing, in: Proceedings of the 27th ICRC, vol. 6, Hamburg, 2001, p. 2119.
[15] R. Brun, F. Bruyant, M. Maire, A.C. McPherson, P. Zanarini, GEANT User's Guide, CERN DD/EE/84-1, Geneva, 1984.
[16] P.A. Aarnio, J. Lindgren, J. Ranft, A. Fassò, G.R. Stevenson, Enhancements to the FLUKA86 program: (FLUKA87), CERN TIS-RP-190, Geneva, 1987.
[17] J.Z. Wang, et al., Cosmic-ray shower simulation and reconstruction for the ATIC experiment, in: Proceedings of the 25th ICRC,vol. 5, Durban, 1997, p. 5.
[18] O. Ganel, E.S. Seo, Adv. Space Res. 26 (11) (2000) 1835.
[19] O. Ganel, et al., Adv. Space Res. 27 (4) (2001) 819.
[20] R. Wigmans, Annu. Rev. Nucl. Particle Sci. 41 (1991) 133.
[21] E.S. Seo, et al., Preliminary results from the first flight of ATIC, in: Proceedings of the 27th ICRC, vol. 5, Hamburg, 2001 p. 1601.
[22] J.P. Wefel, et al., The ATIC science flight in 2002-03: description and preliminary results, in: Proceedings of the 28th ICRC, vol. 4, Tsukuba, 2003, p. 1849, and references therein.